Chapter IV

Results and Discussions

4.1 Mechanical Alloying

Iron and silicon powders weighted to a nominal composition of $FeSi_2$ were milled together by the mechanical alloying process in the argon atmosphere using the planetary ball mill. The total mass is 15.00 g per batch. Small quantity of the mixture in the same batch was taken at different times to be analyzed by XRD. The PDF (Powder Diffraction File) database was used to identify phases of mixture.

PDF NUMBER	**Materials**	**x-ray λ (A°)**	**2θ of a maximum intensity peak degree**
80-0018	Si	1.54060	28.652
06-0696	Fe	1.54050	44.671
20-0532	β-$FeSi_2$	1.54050	29.061 29.158
76-1748	ε-FeSi	1.54060	45.361
73-1843	α-Fe_2Si_5	1.54060	17.279

Table 4.1: Information of the PDF database used for the phase identification

XRD analysis as a function of milling time is presented in Figure 4.1.

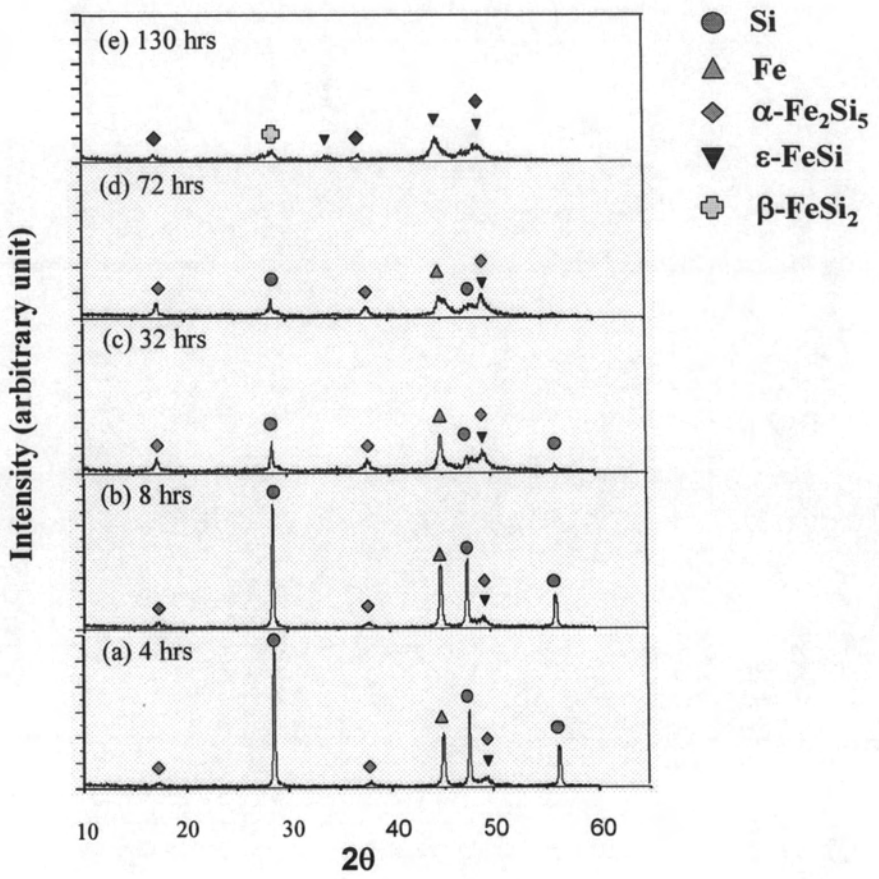

Figure 4.1: XRD pattern of mixture powder after MA process ; (a) 4 hrs, (b) 8 hrs, (c) 32 hrs, (d) 72 hrs and (e) 130 hrs

In Figure 4.1, the elemental Si and Fe peaks appeared with high XRD intensity for 4 and 8 hours of milling and start to decrease after 32 hours of milling. XRD pattern of 72 and 130 hours are almost the same. The decrease in the peak intensity indicates the reduction of crystalline solids size and change into the amorphous state by the mechanically stress-induced disorder with intense milling. The β-$FeSi_2$ peaks appears after of milling 130 hours as shown in Figure 4.1(e). However the element of Si and Fe peaks still remained. In this experiment we would use the milling time for 50 hours and this helps minimize the material preparation time.

4.2 Particle Size Distribution

Particle size distribution of the milled powder for various milling times, is presented in Figure 4.2.

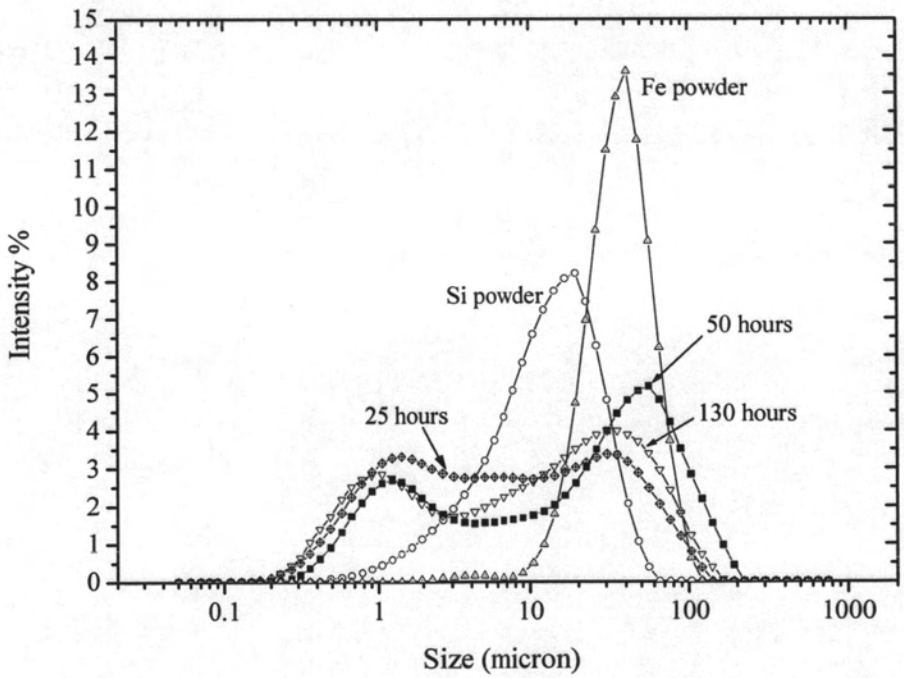

Figure 4.2: The histogram of particles size distribution of Fe + Si mixture for various milling times

As purchased Si and Fe powders have different approximated particle size. From Figure 4.2, the majority sizes of Si and Fe are 14 and 40 μm respectively. After 25 hours of milling, the process approximately reaches a steady state in which welding and fracturing are in balance. Milling time of 25, 50 and 130 hours have approximately similar particle size distribution. Each distribution can be divided into 2 groups. One group is around 1 μm and the other in the range of 20-80 μm.

4.3 Heating Treatment

XRD analysis of heat-treated $FeSi_2$ sample for 3 hours at 1100°C, 10 minutes at 900°C and 10 minutes at 800°C are presented in Figure 4.3.

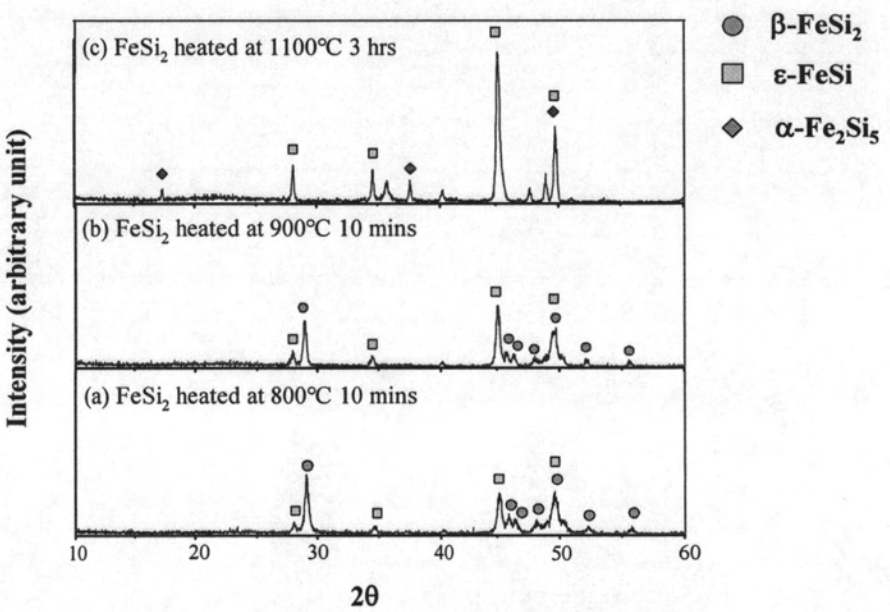

Figure 4.3: XRD patterns of $FeSi_2$ heated at different temperatures

Phases of iron-silicon powder after heating can be either α-Fe_2Si_5, ε-FeSi or β-$FeSi_2$. After heating to 1100°C for 3 hours, α-Fe_2Si_5 and ε-FeSi are observed, as shown in Figure 4.3(c). This is the expected result according to the phase diagram [3]. The heating at 1100°C led to α-Fe_2Si_5 and ε-FeSi formation. Thus, heating at 800-900°C is considered to induce the transformation of β-$FeSi_2$. In this thesis, we choose heating temperature at 900°C for all samples.

Sample with difference Co compositions ($Fe_{1-x}Co_xSi_2$, x = 0.01, 0.03, 0.05) were heated at 900°C for 4 hours and the XRD analysis showed very small β-$FeSi_2$ peak intensity.

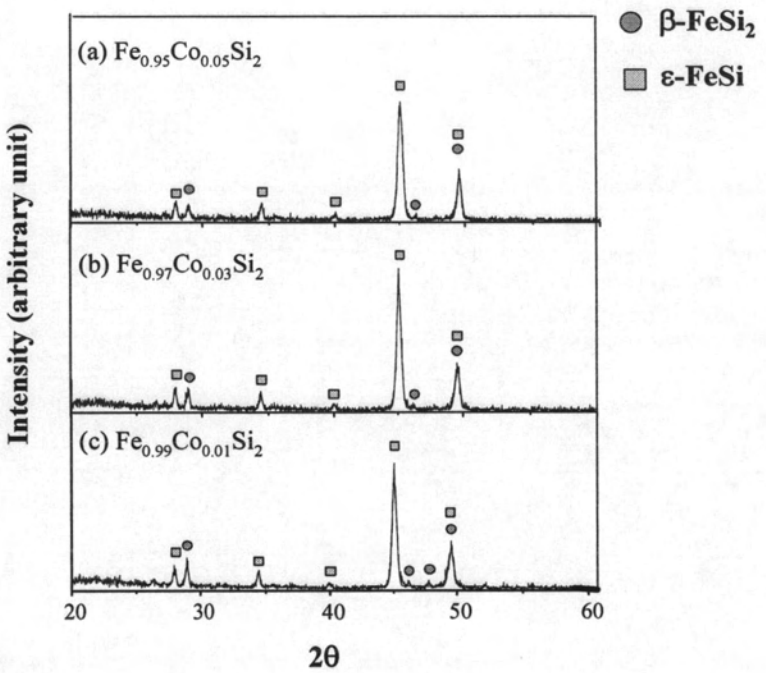

Figure 4.4: XRD pattern of sample (a) $Fe_{0.95}Co_{0.05}Si_2$ (b) $Fe_{0.97}Co_{0.03}Si_2$ and (c) $Fe_{0.99}Co_{0.01}Si_2$ after heating at 900°C for 4 hours

XRD pattern of all samples in Figure 4.4 are similar. The principle peak ratio [I_β/I_ε] was plotted as a function of various Co doping which is shown in Figure 4.5. The principle peak ratio [I_β/I_ε] decreased with an increasing Co doping. It is considered that more Co addition in sample lessens the existence of β-$FeSi_2$ phase. It may be attributed to the fact that Co addition also depresses the transformation Si + ε-FeSi → β-$FeSi_2$ [8].

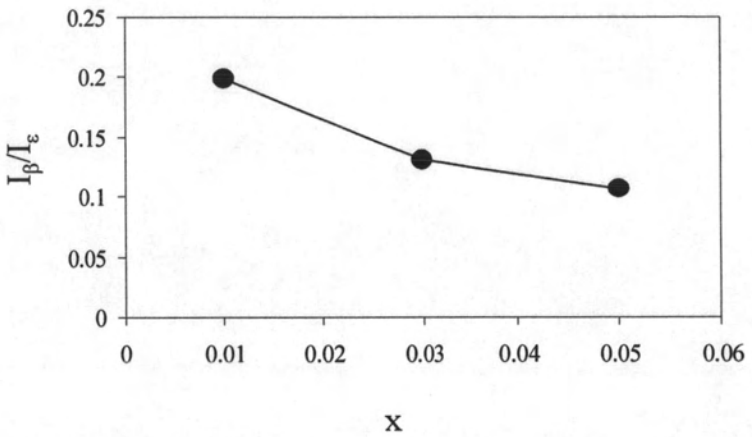

Figure 4.5: The principle peak ratio [I_β/I_ε] where I_β (2 2 0) and I_ε (2 1 0) are principle peak intensity for β and ε phase, respectively

The effect of varying heating time to the phase transformation in $Fe_{0.95}Co_{0.05}Si_2$ is shown in Figure 4.6. It can be seen that the formation of β-$FeSi_2$ and ε-FeSi in $FeSi_2$ and $Fe_{0.95}Co_{0.05}Si_2$ occur at 900°C for 10 minutes heating time. For longer heating times of 1, 2 and 4 hours, β-$FeSi_2$ disappears but the formation of ε-FeSi is still appearance. This has disagreed with Ref [5] which found that longer heating time (or "sintering") for 4-96 hours produced fully transformation to β-$FeSi_2$. However, the literature used a hot-pressed iron-silicide at 1100°C which consist of the untransformed mixture of α-Fe_2Si_5 and ε-FeSi. Thus, subsequent isothermal sintering at proper temperature is considered to be necessary in order to induce the low-temperature transformation of β-$FeSi_2$, and the sintering has been carried out at 830°C for 4-96 hours. The XRD analysis after the isothermal sintering revealed that progressive β-$FeSi_2$ transformation from α-Fe_2Si_5 and ε-FeSi took place along with the annealing time. It was clearly shown that ε-FeSi phases diminished along with annealing time, indicating the progressive peritectoid reaction from α-Fe_2Si_5 and ε-FeSi to β-$FeSi_2$.

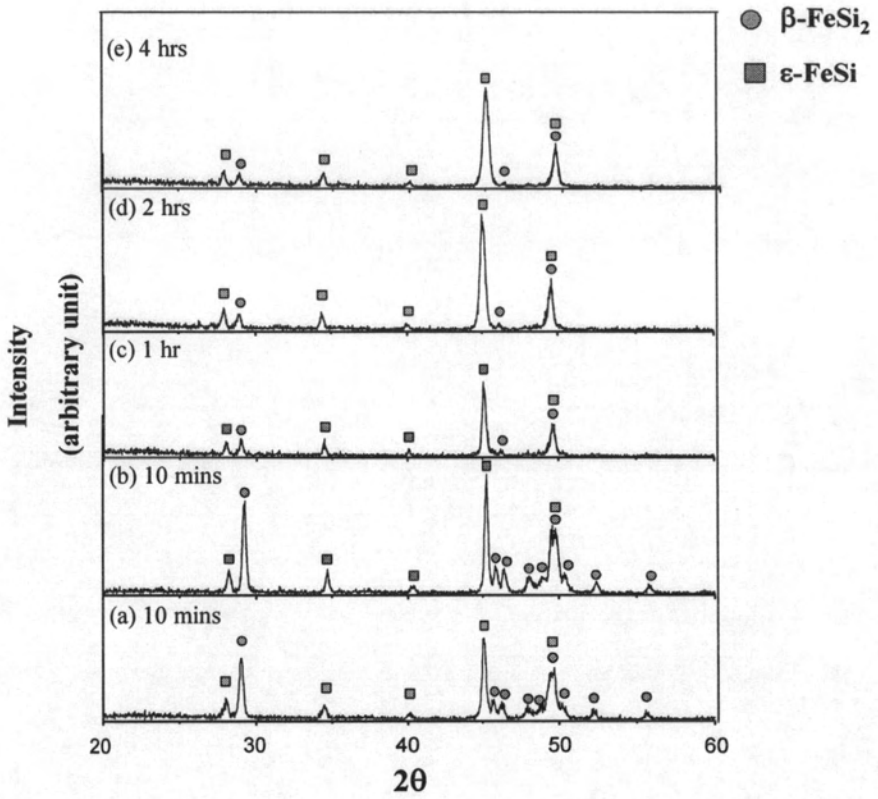

Figure 4.6: XRD pattern of sample (a) $FeSi_2$, (b)-(e) $Fe_{0.95}Co_{0.05}Si_2$ after varies time of heating at 900°C

The principle peak ratio I_β/I_ε decreases with increasing heating time, for 900°C which is shown in Figure 4.7. It is believed that the amount of β-$FeSi_2$ diminish along with heating time because of the unstability of β-$FeSi_2$ phase. Some Si may also be lost during mechanical alloying. From the Si + ε-FeSi → β-$FeSi_2$, missing silicon atoms shifts the sample's composition to the Fe-rich side. Thus the composition shifts is considered to result in an increase in the amount of the ε phases. In some literatures [8,10] excess Si content is added to compensate the Fe contamination which can not be avoided in the powdering process by the iron stamp and the iron ball mill, or to compensate the Si which is lost in the process of sample preparation.

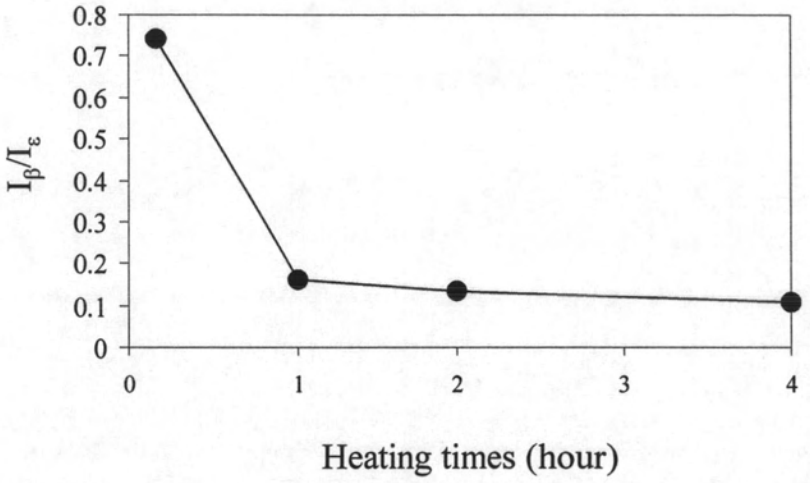

Figure 4.7: The principle peak ratio [I_β/I_ε] of heating $Fe_{0.95}Co_{0.05}Si_2$ samples. I_β (2 2 0) and I_ε (2 1 0) are principle peak intensity for β and ε phase, respectively

4.4 Density

After compacting powder with a hydraulic press at room temperature, the green density is about 2.5 g/cm^3. The density of β-$FeSi_2$ single crystal [3] is 4.93 g/cm^3. It indicates the nearly 50% of sample are porous. Compression under the gauge pressure of 400 MPa for 2 minutes seem insufficient. The density of sample as a function of heating time is shown in Figure 4.8. It shows that the density of heated sample decreased with increasing heating time. Volume of sample increased by 27-80 % with increasing heating time as shown in Figure 4.9. The explanation could probably be due to the relaxation of mechanical stress within the samples. During high energy ball mill, the reduction of crystallite size involved mechanical stress-induced disorder with intense milling [12]. This has been confirmed by an increasing lattice parameter. In addition, observed by SEM (see Section 4.6).

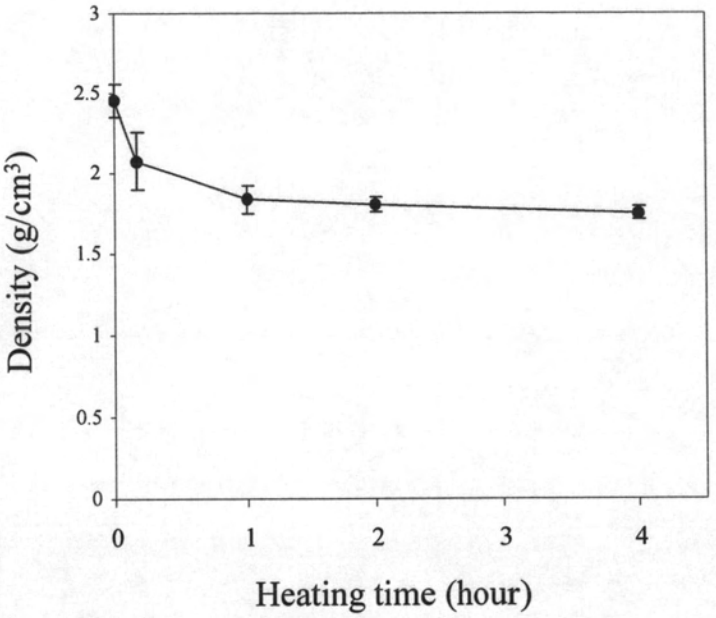

Figure 4.8: Density of sample as a function with heating time

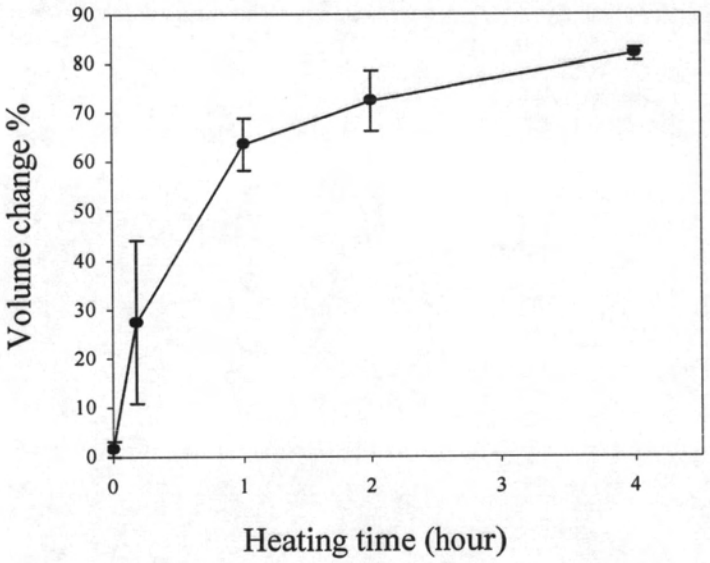

Figure 4.9: The volume change as a function of heating time

4.5 Lattice Parameter

The structure of ε-FeSi is cubic which have lattice parameter of single crystal are $a = b = c = 4.467$ A°. Lattice parameter a is related to the d-spacing (d) by [13]

$$\frac{1}{d^2} = \frac{h^2 + k^2 + l^2}{a^2} \tag{4.1}$$

where (h k l) is plane of crystalline. We used (h k l) of (1 1 0), (1 1 1), (2 1 0) and (2 1 1) from PDF number 76-1748 whose peaks are at 2θ of 28.230°, 34.757°, 45.361° and 49.972° respectively. The d-spacing (see Section 3.2.1) values of our samples in XRD pattern is shown in Table 4.2.

d-spacing at (1 1 0) A°	d-spacing at (1 1 1) A°	d-spacing at (2 1 0) A°	d-spacing at (2 1 1) A°	Time of heating
3.1631	2.5802	1.9998	1.8270	10 minutes
3.1796	2.5976	2.0097	1.8338	1 hour
3.1902	2.6046	2.0133	1.8364	2 hours
3.2009	2.6035	2.0120	1.8368	4 hours

Table 4.2: Table of d-spacing values at (1 1 0), (1 1 1), (2 1 0) and (2 1 1) of time heating is 10 minutes, 1 hr, 2 hrs and 4 hrs

We used ε-FeSi phase to calculate lattice parameter, because of β-$FeSi_2$ phase disappeared and ε-FeSi still appeared when enhance heating time. Lattice parameter as a function of heating time is shown in Figure 4.10. Lattice parameter increased with increased heating time which determined using the XRD patterns. Heating 900°C from 0 hour to 4 hours, lattice parameter enhanced 1 % which increased volume of sample. Increasing of volume has 2 compound are porous and volume of material.

This result decreases the density of sample. Green density is about 2.5 g/cm^3 which shows nearly 50 % of porous and 50 % of material. Heating 4 hours the density is 1.75 g/cm^3 which shows 65 % of porous. It indicates the porous enhance 15 %. From calculation, volume of material enhanced 32 %.

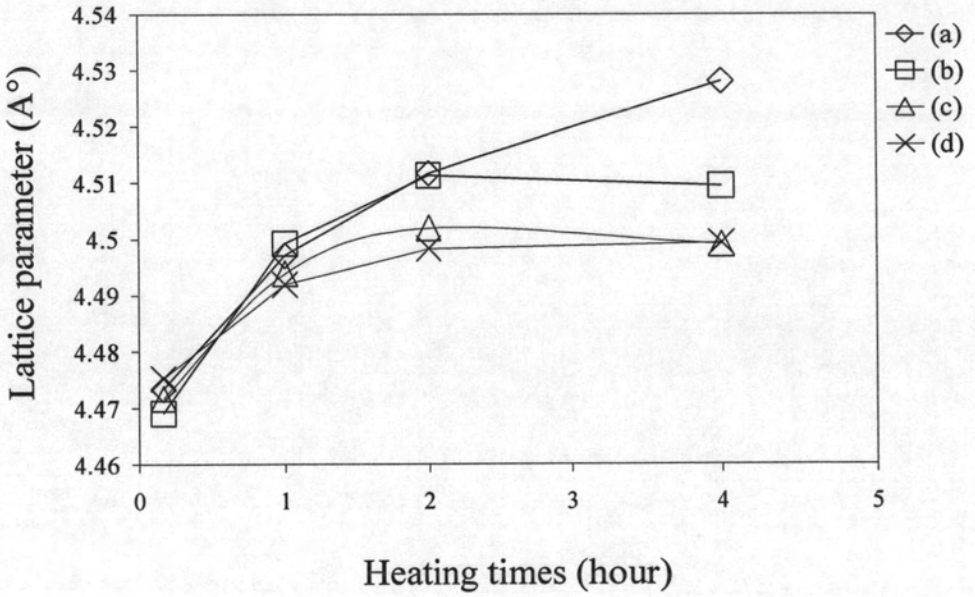

Figure 4.10: Lattice parameter *a* as a function with heating time at (a) (1 1 0), (b) (1 1 1), (c) (2 1 0) and (d) (2 1 1). Line are the guidances to the eyes.

4.6 Scanning Electron Microscopy (SEM)

The SEM micrographs of heated $Fe_{0.95}Co_{0.05}Si_2$ sample for 10 minutes and 4 hours are presented in Figure 4.11. Heat for 10 minutes sample formed small agglomeration, which consisted of average particles size is 0.57 ± 0.180 μm. For heating 4 hours, it consisted of higher agglomeration with more spherical in shape which consisted of average particle size is 0.65 ± 0.236 μm. It can be seen that the sintering process did not happen fully and the average size is not significantly different. The Figure 4.11 (a)-(b) represent SEM micrograph which change region to

take photograph. All SEM photograph of heated at 900°C for 10 minutes and 4 hours have similarly figure.

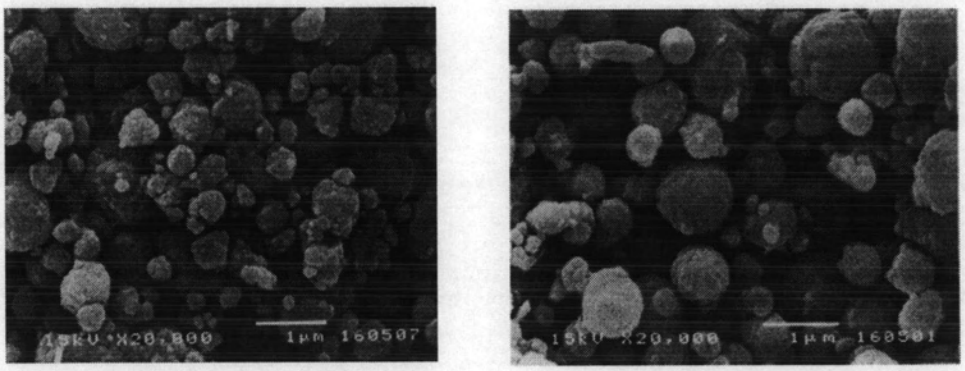

(a) 10 minutes (b) 4 hours

Figure 4.11: SEM of $Fe_{0.95}Co_{0.05}Si_2$ sample heating 900°C for (a) 10 minutes, (b) 4 hours

4.7 Binder Effect

Binder was added to the mixed powder for increasing the green strength, particle packing and avoid cracking. The binder consists of 0.12 % by weight (0.086 % of Toluene, 0.022 % of Ethanol, 0.012 % of Ethyl Cellulose). After MA and cold-press, the green density is 2.26 g/cm^3. Heating samples for 1 hour at 500°C was employed to burn out the binder before a next heated sample at 900°C for a soaking time of 10 minutes. The density of heat-treated sample is 2.21 g/cm^3. Therefore, the added binder did not increase density. From the Figure 4.12, XRD pattern of sample with added binder and no added binder show the same patterns. This implies that the binder has no effect on the phase transformation.

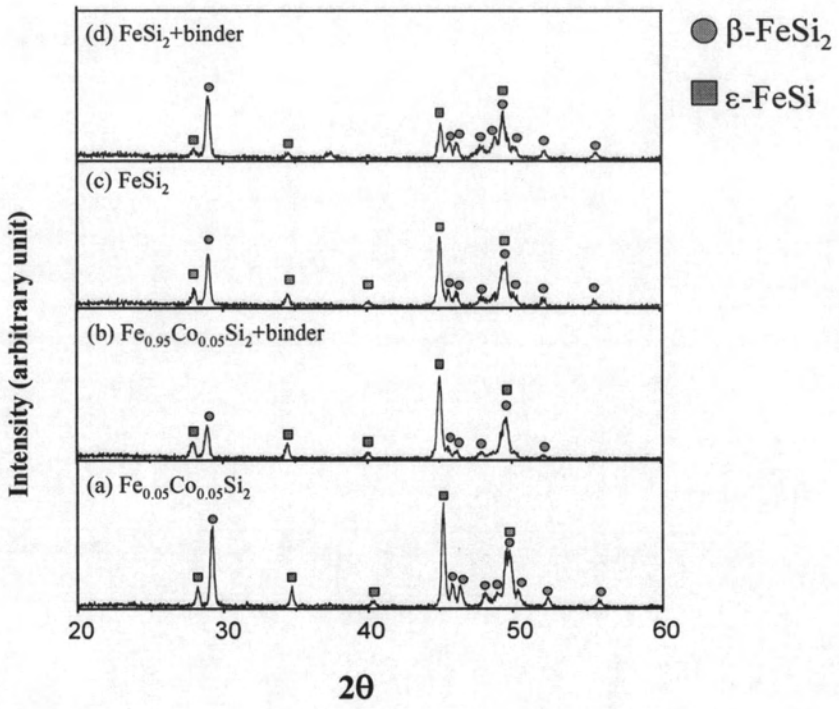

Figure 4.12: XRD pattern of sample after heating at 900°C for 10 minutes with added and non-added binders

Figure 4.13 shows XRD of several samples prepared with different methods of heating. XRD pattern in Figure 4.13(a) is $FeSi_2$ which was heated at 900°C for 10 minutes. It consisted of β-$FeSi_2$ and ε-FeSi. Next this sample was milled to powder and binder was added and mixed it together by a mortar. After compacting of the powder, heating at 900°C for 10 minutes was repeated but this time the sample was buried under the $FeSi_2$ powder. The objective of this method was to prevent reaction of sample with the surrounded environment. Powder of $FeSi_2$ might react with the surface of buried sample. Figure 4.13(c) shows XRD pattern consisting of β-$FeSi_2$ and ε-FeSi which are the same as the XRD pattern in Figure 4.13(a) and 4.13(b). Next method was to add binder to $FeSi_2$ powder and mixed it together. After compacting, sample was heating at 900°C for 10 minutes and buried underneath $FeSi_2$ powder. XRD pattern in Figure 4.13(d) shows only β-$FeSi_2$ peaks without ε-FeSi which is

remarkable. In normal heating method we don't bury sample with $FeSi_2$ powder and the sample consisted of β-$FeSi_2$ and ε-FeSi phases. It is expected that when the sample buried with $FeSi_2$ powder, Si from the powder may compensate Si in the sample which otherwise lost during preparation.

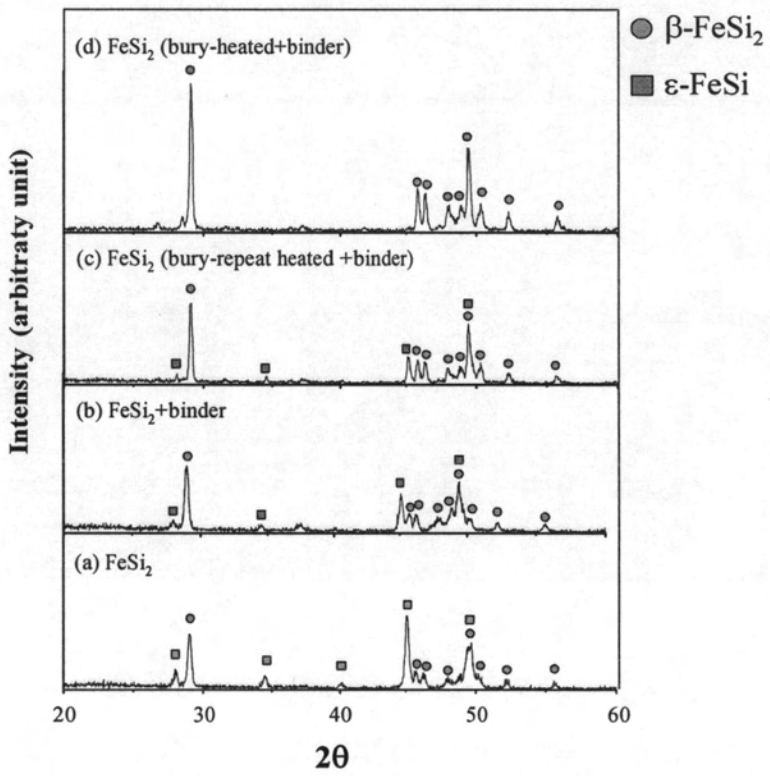

Figure 4.13: XRD pattern of heating sample at 900˚C for 10 minutes

4.8 Thermopower

Figure 4.14 shows the thermopower of $FeSi_2$, $Fe_{0.97}Co_{0.03}Si_2$ and $Fe_{0.95}Co_{0.05}Si_2$ heated at 900˚C for 10 minutes as a function of temperature in the range 25-525˚C.

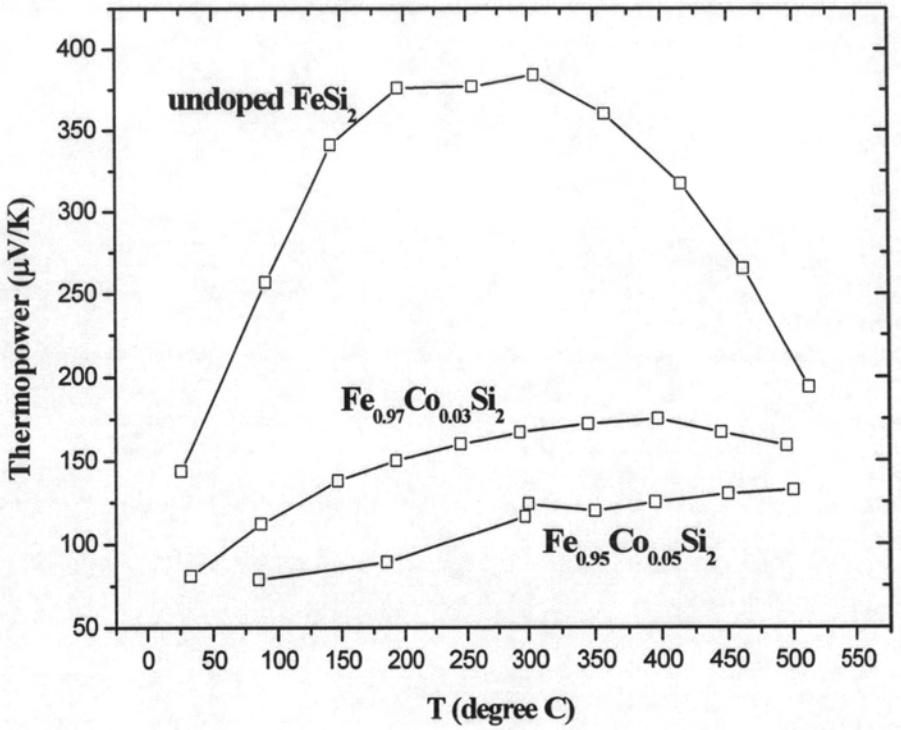

Figure 4.14: Thermopower of $FeSi_2$, $Fe_{0.97}Co_{0.03}Si_2$, $Fe_{0.95}Co_{0.05}Si_2$

The thermopower of non-doped $FeSi_2$ increased in the temperature range 25-175°C and decreased above 300°C. The maximum thermopower is 375 μV/K at 300°C. Increasing Co doping content, the peak position shifted toward higher temperatures. The maximum thermopower of $Fe_{0.97}Co_{0.03}Si_2$ is 175 μV/K at 400°C and $Fe_{0.95}Co_{0.05}Si_2$ is 130 μV/K at 500°C. Sample with high Co doping has less thermopower because of the less amount of β-$FeSi_2$. ε-FeSi is metallic which has small thermopower. The thermopower depends on the carrier concentration in such a way that increasing carrier concentration decreases the thermopower, following the expression derived by Cutler and Mott (1969) [14]

$$\alpha_N = -\frac{k_B}{e}[\ln(N_C / n) + A] \tag{4.2}$$

$$\alpha_P = +\frac{k_B}{e}[\ln(N_V / n) + A] \tag{4.3}$$

α_N and α_P are the N-type and P-type thermopower, respectively. A depends on how the carrier mobility varies with energy in a band. It is usually smaller than the first term and can be neglected. N_C *and* N_V is the effective densities of states in conduction and valence bands. n is carrier concentration.

The carrier concentration as a function of temperature is schematically shown in Figure 4.15.

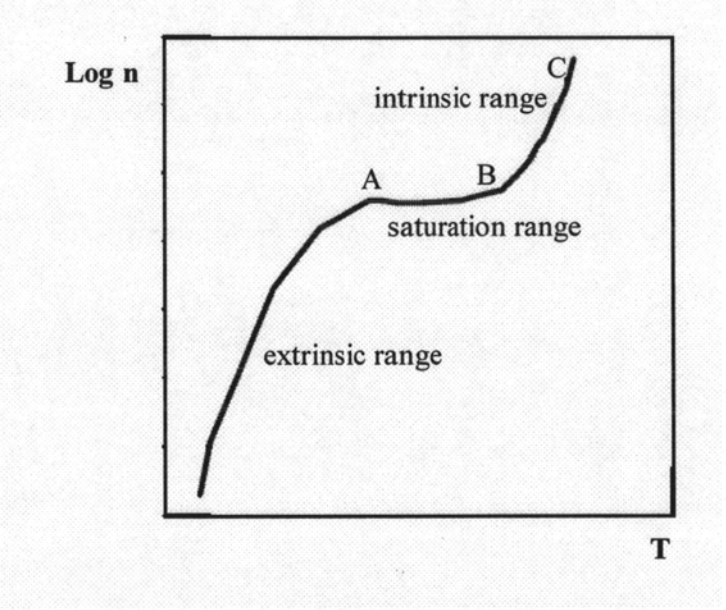

Figure 4.15 : Carrier concentration as a function with temperature

From our experiment, we heated sample from 25 to 525°C which increased thermopower in range 25-300°C, 25-400°C and 75-500°C for $FeSi_2$, $Fe_{0.97}Co_{0.03}Si_2$ and $Fe_{0.95}Co_{0.05}Si_2$ respectively. This is because N_c increases proportionally with $T^{3/2}$ while n is approximately constant (range A-B). The thermopower decreases when

heat sample over 300-400°C. Decreasing thermopower with increasing temperature can be explained from Equation (4.2) and (4.3) that n increases exponentially while N_c increases at slower rate (See B-C range).

4.9 Resistivity

In Figure 4.16 we plot the logarithm of electrical resistivity of the $Fe_{1-x}Co_xSi_2$ for x = 0, 0.03, and 0.05 as a function of temperature in the range of 75-525°C.

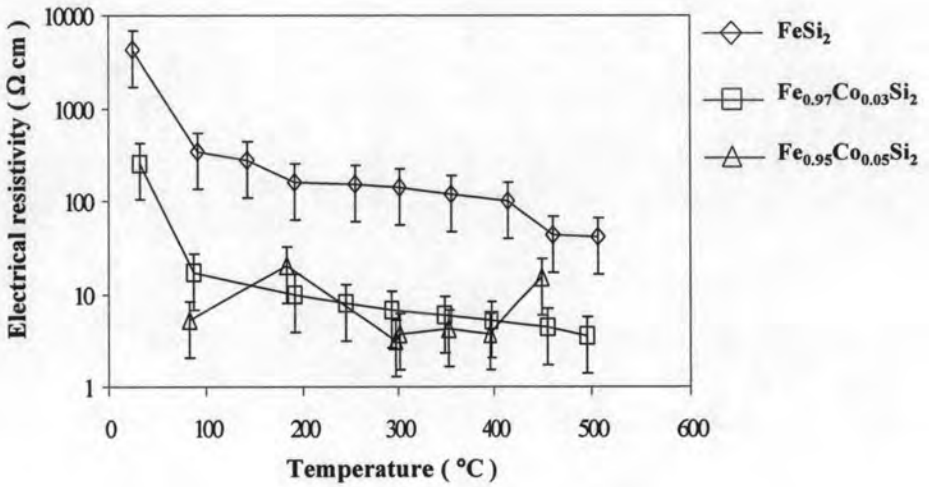

Figure 4.16: Electrical resistivity of sample as a function with temperature

The electrical resistivity of all samples decreased with increasing temperature, indicating a semiconductor behavior. The electrical resistivity decreased with increasing Co contents, it supply more charge carriers which reducing the electrical resistivity. A correction factor G can be calculated by

$$G = \frac{2\pi s}{F} \tag{4.4}$$

$$F = \left(\frac{a}{s}, \frac{h}{s}, \frac{l}{s}\right) \tag{4.5}$$

The values of F for an infinitely long bar are shown in Figure 3.5. The spacing of prob (s) is ~ 1mm.

4.10 Power Factor

The thermopower and electrical resistivity of all samples were measured at room temperature up to 525°C. From electrical resistivity and thermopower, we can calculate the thermoelectric power factor of sample from $\alpha^2\sigma$. The temperature dependence of the power factor for each of sample is shown in Figure 4.17. The power factor of $FeSi_2$ and $Fe_{0.95}Co_{0.05}Si_2$ increased up to 0.001574 – 0.004006 $\mu W/K^2cm$ and then decreased with temperature. Because of the carrier concentration was increased by temperature which is decreased thermopower. Power factor of $Fe_{0.97}Co_{0.03}Si_2$ are still regarded to be high with increase temperature. M. Ito and co worker [15] arc-melted the mixtures of Fe and Si powders to form a button. The buttons were pulverized to -60 mesh using a mortar. These powders were MA for 20 hours and hot-pressed at 900°C for 1 hour under 25 MPa. They report the power factor at room temperature up to 900°C. The maximum power factor of $FeSi_2$ and $Fe_{0.98}Co_{0.02}Si_2$ are 0.35 and 2.75 $\mu W/K^2cm$ at 250°C and 300°C respectively.

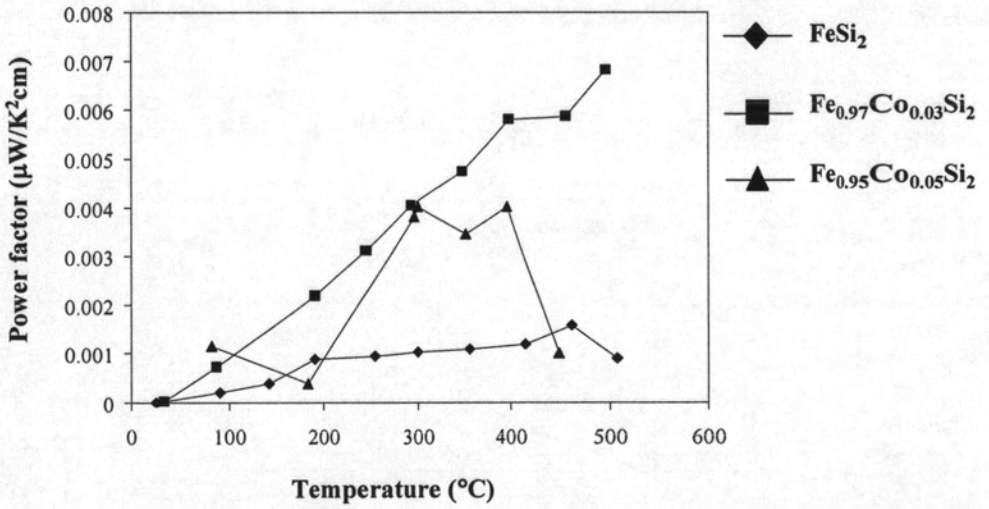

Figure 4.17: Power factor of sample as a function of temperature

4.11 Room Temperature Thermopower

Example of the thermopower on $Fe_{0.95}Co_{0.05}Si_2$ heat-treatment at 900°C for 10 minutes measured at room temperature in the air is shown in Figure 4.18.

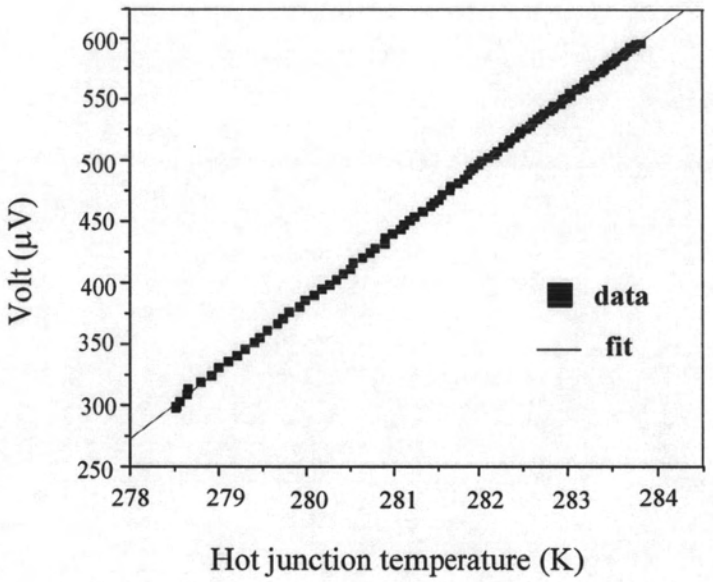

Figure 4.18: Example of thermopower measurement of $Fe_{0.95}Co_{0.05}Si_2$ heated at 900°C for 10 minutes

The average thermopower in Figure 4.18 of $Fe_{0.95}Co_{0.05}Si_2$ is 55.29 μV/K at room temperature. All samples which were heated at 900°C for 10 minutes have a similar order of magnitude thermopower. The thermopower of non-doped $FeSi_2$ is about 120 μV/K. The thermopower of $Fe_{0.99}Co_{0.01}Si_2$, $Fe_{0.97}Co_{0.03}Si_2$ and $Fe_{0.95}Co_{0.05}Si_2$ are 65 μV/K, 100 μV/K and 70 μV/K respectively. Difference of thermopower values can be explained in term of different amount of β-$FeSi_2$, α-Fe_2Si_5 and ε-FeSi, each has the thermopower of 250, 10 and 2.6 μV/K respectively [16]. Samples with heat treatment at 900°C for 1, 2 and 4 hours produce thermopower in a range of 5-15 μV/K, because of very small amount of β-$FeSi_2$ (See Figure 4.6). The Figure 14.19 (a) show β-$FeSi_2$ phase depressed by the increase in Co content.

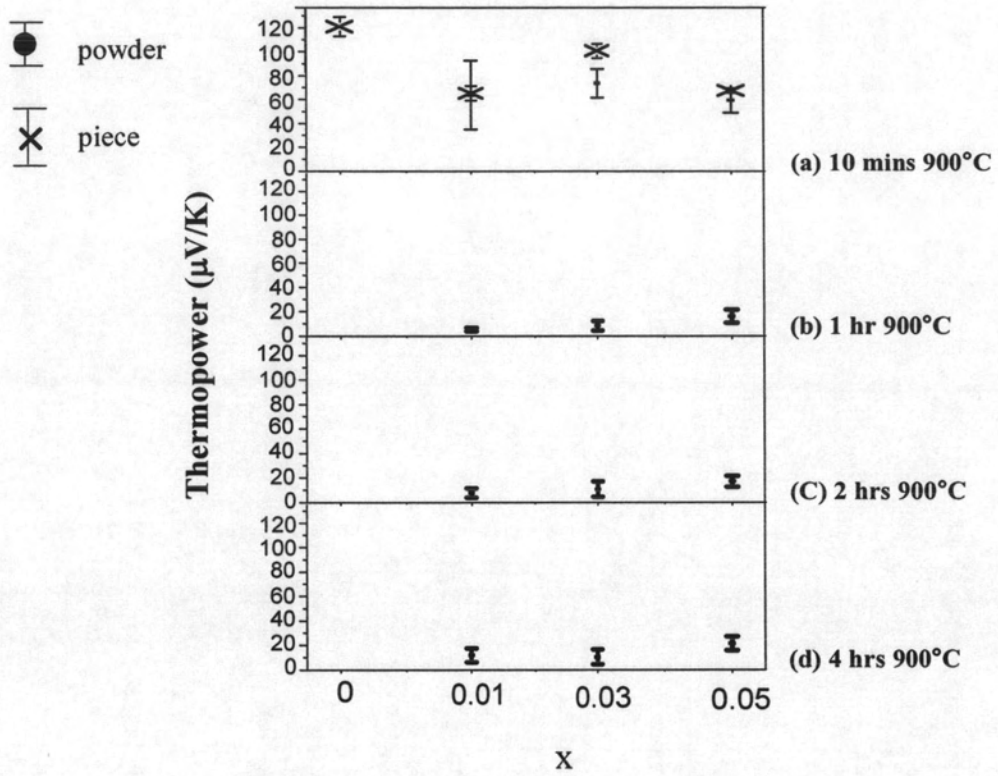

Figure 4.19: Room temperature thermopower of various $Fe_{1-x}Co_xSi_2$ heat-treatment at 900°C for 10 mins, 1 hr, 2 hrs and 4 hrs

Our samples have both β-$FeSi_2$ and ε-FeSi which includes thermopower of two phases. The thermopower can calculated by [17]

$$\alpha = \frac{\sigma_\beta \alpha_\beta + \sigma_\varepsilon \alpha_\varepsilon}{\sigma_\beta + \sigma_\varepsilon} \tag{4.6}$$

If we approximate σ_β and σ_ε by I_β and I_ε assuming that the mobility of β-$FeSi_2$ and ε-FeSi are the same and the intensity is proportional to the carrier density, we obtain

$$\alpha = \frac{\frac{I_\beta}{I_\varepsilon}\alpha_\beta + \alpha_\varepsilon}{\frac{I_\beta}{I_\varepsilon} + 1}. \qquad (4.7)$$

From Figure 4.7, the principle peak I_β/I_ε decrease with increasing heating time. Figure 4.20 shows the thermopower versus I_β/I_ε. Thermopower from the experiment is less than that from the theory (α_β = 250 μV/K, α_ε = 2.6 μV/K). This indicates that ε-FeSi and β-$FeSi_2$ in our sample have poorer quality than those in a single crystal forms. The sintering process didn't happen fully.

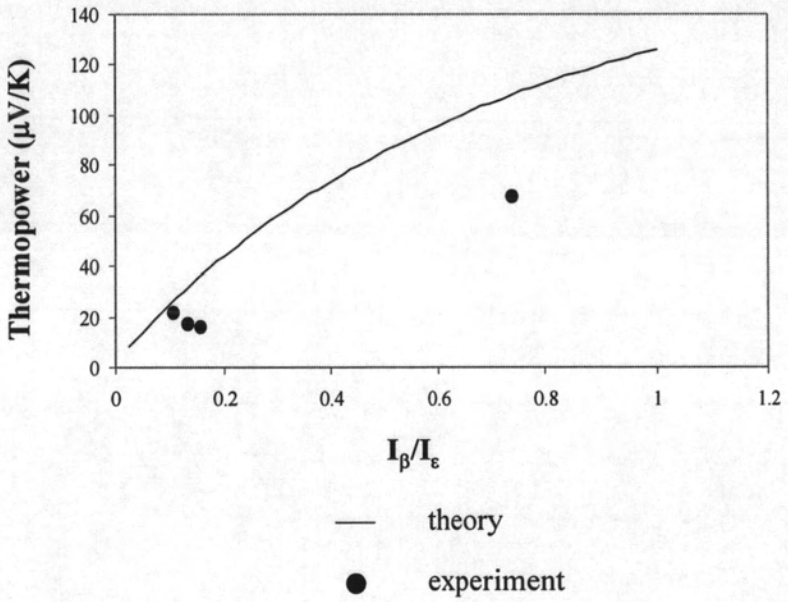

Figure 4.20: Thermopower of $Fe_{0.95}Co_{0.05}Si_2$ as a function of I_β/I_ε

4.12 Room Temperature Hall Effect

4.12.1 Carrier Concentration

Hall effect measurements confirm an increase of carrier concentration with increasing Co content. Because van der Pawn method is applied to the two-dimensional flow of the current, the samples are there grinded to the thickness of 0.3 mm by a sandpaper to check the consistency of the result. The carrier concentration of $Fe_{0.95}Co_{0.05}Si_2$ less than $Fe_{0.97}Co_{0.03}Si_2$ and $FeSi_2$ which is not follow theory. This result is may be occurred impurity by the process of preparation from glue and sandpaper.

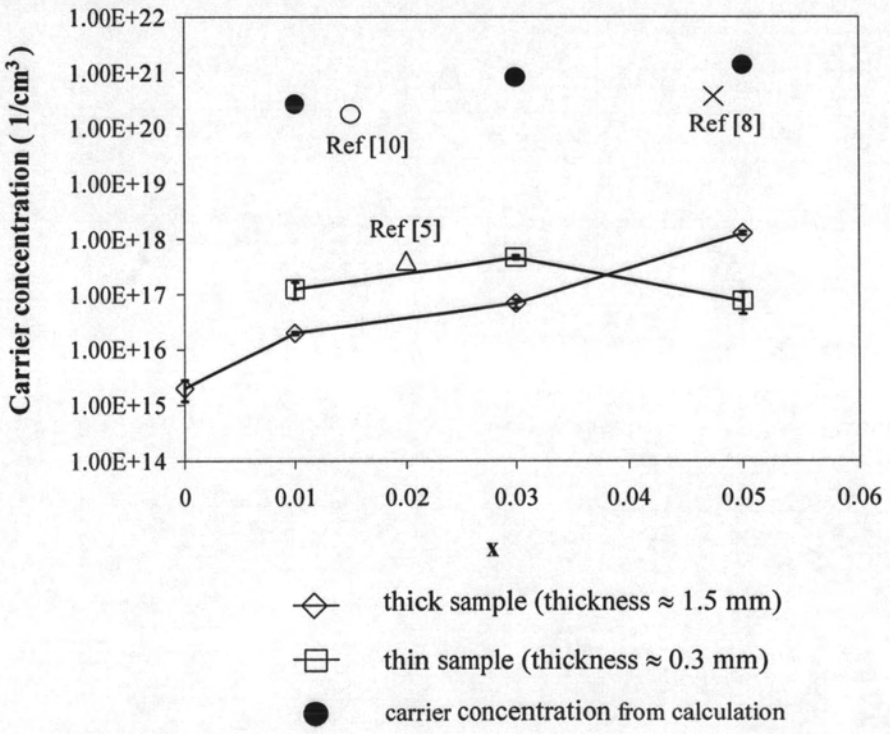

Figure 4.21: The Hall carrier concentration of $Fe_{1-x}Co_xSi_2$ heat-treated at 900°C for 10 minutes

The carrier concentration result is lower than that reported in literature [5, 8, 10]. It implies that the ionization of Co-dopant occur to the less extend which might indicate imperfection of doping process where Fe atom should have been substituted by Co atom. The carrier concentration from calculation is shown in Figure 4.21. It may be an interstitial point defect. The interstitial is a normal lattice atom displaced from its normal position, or it can be a foreign atom [18].

4.12.2 Mobility

The mobility (μ) at room temperature is 14.97 cm^2/Vs for x = 0, 28.82 cm^2/Vs for x = 0.01, 87.53 cm^2/Vs for x = 0.03 and 20.2 cm^2/Vs for x = 0.05. The mobility of thin sample varies about 2-6 cm^2/Vs which is shown in Figure 4.22.

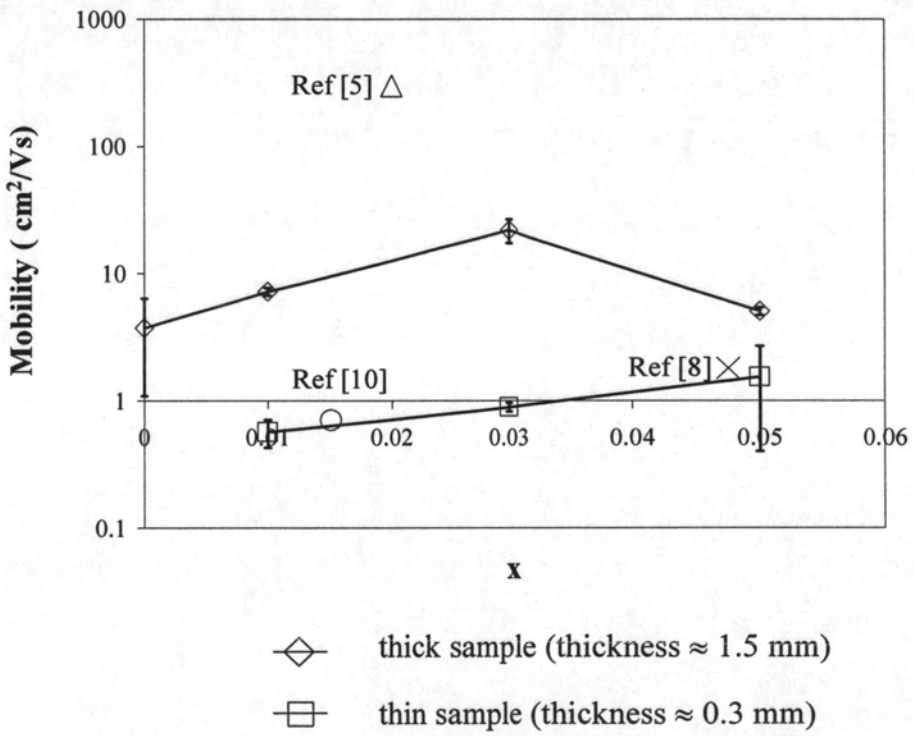

Figure 4.22: Mobility of samples as a function with Co content

Our thick samples have mobility higher than reference because samples of reference have higher carrier concentration than that of literature and this is because samples of

reference have higher carrier concentration than our sample. It effects of additional carrier scattering mechanism which is reduced the carrier mobility.

4.12.3 Electrical Resistivity

The logarithm of electrical resistivity by van der Pauw method at room temperature decrease with increasing Co content as shown in Figure 4.23 for normal thickness (d = 1.5 mm). The resistivity of thin sample varies between 10 Ω cm and 100 Ω cm.

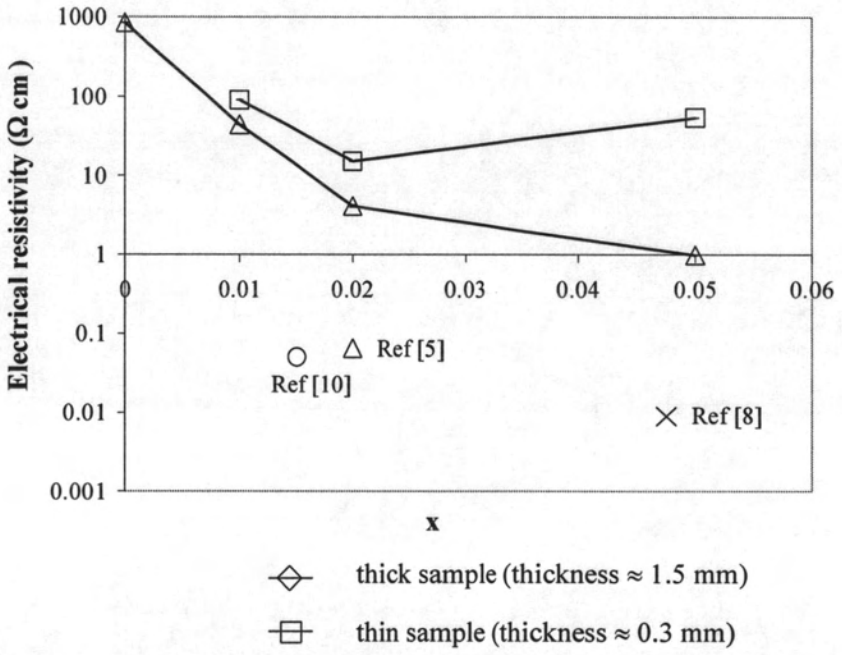

Figure 4.23: Electrical resistivity of samples as a function of Co content

The electrical resistivity of our samples is higher than that of the literature, because the carrier concentration of our samples less than of the reference.

4.12.4 Power Factor

Power factor at room temperature was calculated for each sample (d = 1.5 mm) which is shown in Figure 4.24. It increases with the increase Co content. The values vary in range 0.000017 – 0.004312 $\mu W/K^2cm$.

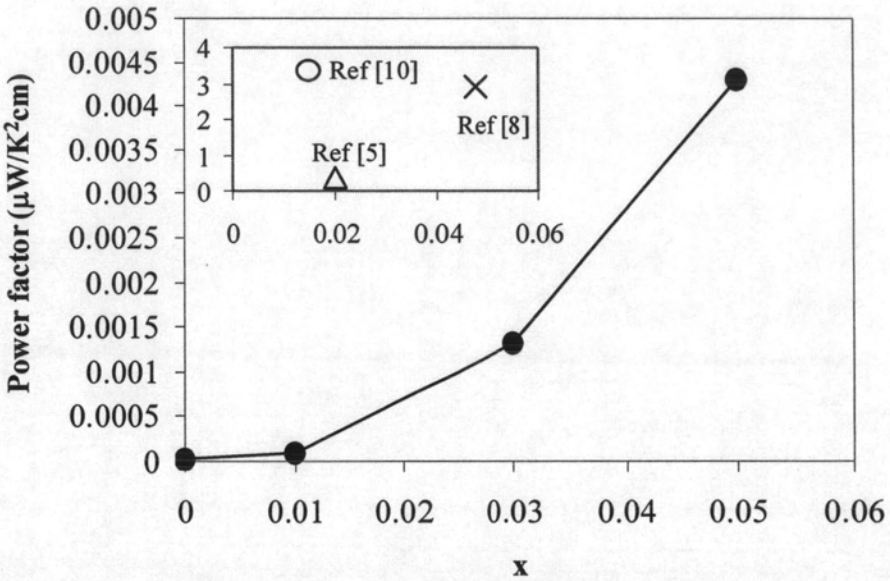

Figure 4.24: Power factor of sample as a function with Co content

x $Fe_{1-x}Co_xSi_2$	Thick (mm)	Type of carrier	ρ (Ω-cm)	R_H	n (cm^{-3})	μ (cm^2/Vs)
0	1.5	electron	842.05	-1.26×10^{-2}	1.98×10^{15}	3.74
0.01	1.5	hole	44.16	1.27×10^{-3}	1.96×10^{16}	7.41
0.03	1.5	hole	4.23	3.70×10^{-4}	6.75×10^{16}	21.88
0.05	1.5	electron	0.98	-1.92×10^{-5}	1.26×10^{18}	5.0497
0.01	0.39	electron	89.57	-2.03×10^{-4}	1.65×10^{17}	5.66×10^{-1}
0.03	0.28	hole	15.17	5.14×10^{-5}	4.27×10^{17}	8.91×10^{-1}
0.05	0.34	electron	53.99	-3.32×10^{-4}	4.23×10^{16}	1.54

Table 4.3: Hall coefficient, carrier concentration and mobility of samples at room temperature

The majority carrier in $Fe_{0.99}Co_{0.01}Si_2$ and $Fe_{0.97}Co_{0.03}Si_2$ with d = 1.5 mm are holes which disagree with the known type of electron. Actually, the thermopower measurement has confirmed to be the n-type carrier. Therefore our Hall measurements are not fully satisfied. Figure 4.25 show I-V characteristic between pairs of two contacts which are non-linear and this might cause the unreliable measurement so far.

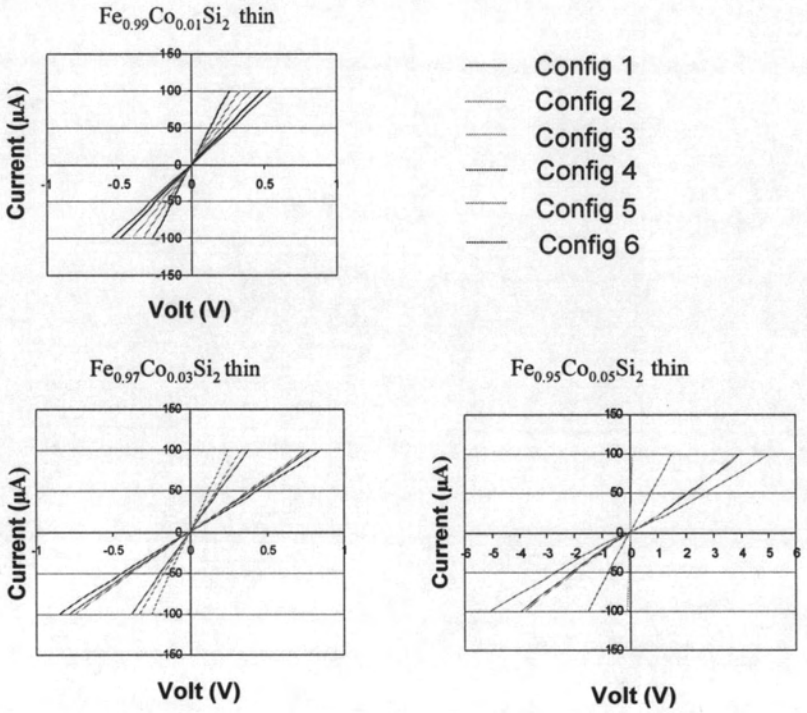

Figure 4.25: The I-V plot of all configurations